Hindawi Publishing Corporation
Advances in Materials Science and Engineering
Volume 2014, Article ID 795384, 8 pages
http://dx.doi.org/10.1155/2014/795384

Research Article

Structural Modification of Sol-Gel Synthesized V_2O_5 and TiO_2 Thin Films with/without Erbium Doping

Fatma Pınar Gökdemir, Ayşe Evrim Saatci, Orhan Özdemir, and Kubilay Kutlu

Department of Physics, Yıldız Technical University, 34220 Istanbul, Turkey

Correspondence should be addressed to Orhan Özdemir; ozdemir@yildiz.edu.tr

Received 29 May 2014; Revised 6 August 2014; Accepted 26 August 2014; Published 13 October 2014

Academic Editor: Somchai Thongtem

Comparative work of with/without erbium- (Er-) doped vanadium pentoxide (V_2O_5) and titanium dioxide (TiO_2) thin films were carried out via sol-gel technique by dissolving erbium (III) nitrate pentahydrate ($Er(NO_3)_3{\cdot}5H_2O$) in vanadium (V) oxoisopropoxide ($OV[OCH(CH_3)_2]_3$) and titanium (IV) isopropoxide ($Ti[OCH(CH_3)_2]_4$). Effect of Er doping was traced by Fourier transform IR (FTIR), thermogravimetric/differential thermal (TG/DTA), and photoluminescence measurements. UV-Vis transmission/absorption measurement indicated a blue shift upon Er doping in V_2O_5 film due to the softening of V=O bond while appearance of typical absorption peaks in Er-doped TiO_2 film. Granule size of the films increased (reduced) upon Er substitution on host material compared to undoped V_2O_5 and TiO_2 films, respectively.

1. Introduction

Titanium dioxide (TiO_2) and vanadium pentoxide (V_2O_5) thin films have drawn considerable attention with their outstanding properties that make them key elements for optical coatings [1], gas sensors [2], electrode materials for Li ion batteries [3], and electrochromic devices [4]. These oxides have also potentials as host materials for rare earth ion implantation due to the suitability of oxygen inclusion and their wide band gap nature that enhance the photoluminescence (PL) emission of dopant ion [5]. Among them, erbium (Er) has a potential interest for telecommunication due to sharp photoluminescence emission at 1540 nm, which corresponds to a minimum loss window for silica optical fibers and ascertains its importance [6]. Additionally, Er doping, especially in TiO_2 film, leads to enhancing photocatalytic activity due to the absorption peaks located at 490, 523, and 654 nm, being attributed to the transitions of 4f electrons from $^4I_{15/2} \rightarrow {}^4F_{7/2}$, $^4I_{15/2} \rightarrow {}^2H_{11/2}$, and $^4I_{15/2} \rightarrow {}^4F_{9/2}$, respectively. Furthermore, red shift in absorption edge of TiO_2 might be observed due to Er doping. Consequently, it is important to investigate how Er ion acts and locates in the network of host material. In this work, we monitored structural changes by Er doping on V_2O_5 and TiO_2 films through UV-Vis transmittance spectroscopy, photoluminescence (PL) measurement, and Fourier transform infrared spectroscopy (FTIR). Additionally, we correlated the charge capacity and structural alteration by Er doping on V_2O_5 and TiO_2 films through cyclic-voltammetry and AFM measurements as well as the surveyed techniques.

2. Experimental

$Ti[OCH(CH_3)_2]_4$ and $OV[OCH(CH_3)_2]_3$ were used as sol precursors. For TiO_2 sol, 2.4 mL of $Ti[OCH(CH_3)_2]_4$ was added to 30 mL ethanol and mixed in a magnetic stirrer for 1 h. 10 mL glacial acetic acid (CH_3CO_2H) and 20 mL ethanol was introduced into the mixture and stirred. Finally, 3 mL triethylamine ($(C_2H_5)_3N$) was added and solution was mixed for 4 h. For V_2O_5 sol, 10.2 mL $OV[OCH(CH_3)_2]_3$ was added into 40 mL isopropyl alcohol ($(CH_3)_2CHOH$) and solution was mixed for 2 h. 1 mL glacial acetic acid was added to the mixture and stirred. Er doping was carried out using $Er(NO_3)_3{\cdot}5H_2O$ powder which was dissolved in TiO_2 and V_2O_5 sols resulting in 0.1 M concentration. Films were deposited on soda lime glass (SLG) and indium tin oxide (ITO) coated glass substrates by dip coating at a

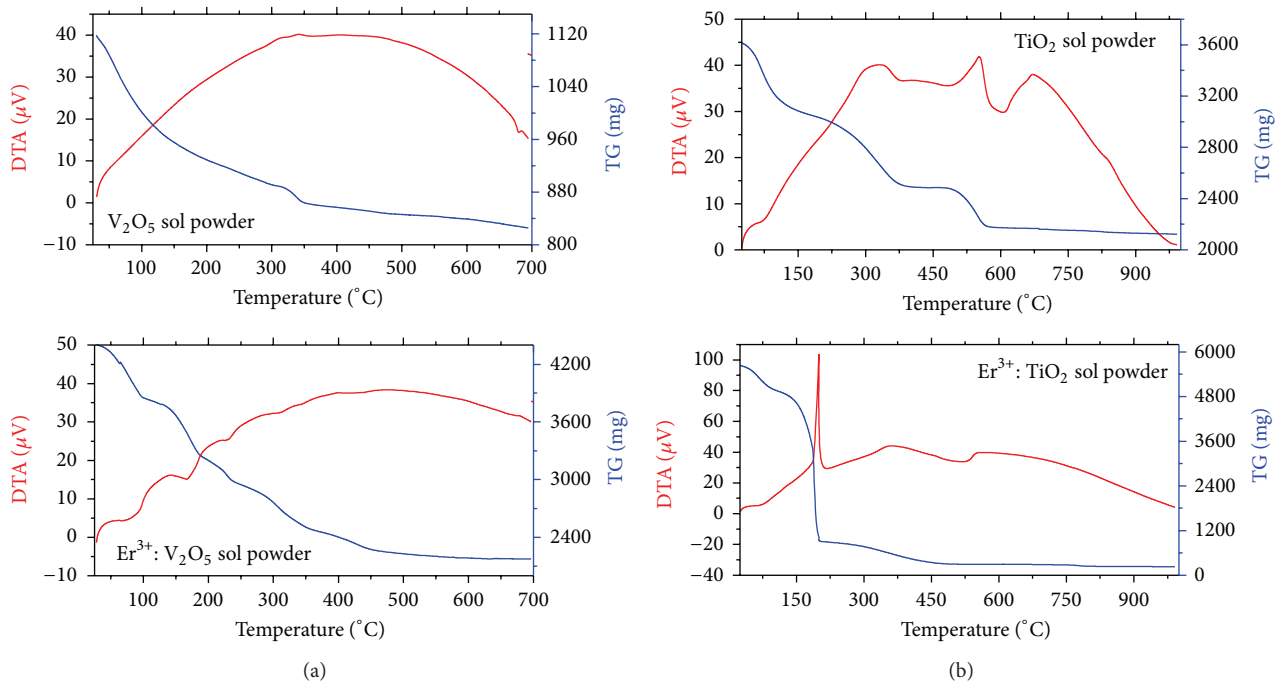

FIGURE 1: TG/DTA curves of the (a) V_2O_5 and (b) TiO_2 coating sol powders.

constant speed of 100 mm/min. Prior to deposition, substrates were cleaned in an ultrasonic bath using acetone, isopropyl alcohol, and deionized (DI) water, respectively. Deposited films were dried at room temperature and then heat-treated at 150°C for 20 min. The processes were resumed for double layer, resulting in uniform films. These sols were allowed to dry in open atmosphere at room temperature and powders were used for TG/DTA analysis, performed with a Seiko SII Exstar 6000 TG/DTA 6300 model using an Al_2O_3 crucible in static air ambient with a heating rate of 10°C/min. FTIR measurement was performed by a Bruker Tensor 27. Transmittance measurements were carried out using a PG Instruments T80 model UV/Vis spectrophotometer. AFM measurements were made with a Park Systems operating at noncontact mode. Electrochemical analyses were carried out using Autolab PGSTAT30 model potentiostat/galvanostat. Photoluminescence measurements were performed at room temperature through a monochromator (Newport 260) equipped with SR830 lock-in amplifier and silicon photodiode. Different light sources as excitation wavelengths were used, resulting in the same feature of PL spectra for the present films.

3. Results and Discussion

TG/DTA experiment was carried out with the temperature range from 25°C to 1000°C for V_2O_5 and TiO_2 powders, respectively. Figure 1(a) showed the first weight loss up to 320°C with a large endotherm, associated with the volatilization and combustion of organic species for undoped V_2O_5 film. Second change occurred around the 343°C, corresponding to the phase transition while other mass losses started at 610°C, reflecting the melting point of V_2O_5. TG/DTA curves of the TiO_2 powder, on the other hand, showed two mass losses that were associated with endothermic and exothermic events and depicted in Figure 1(b). The first endothermic event took place around 90°C, denoting elimination of water while exothermic events were due to the volatilization and combustion of CH_3OH, $(CH_3)_2CHOH$, and CH_3COOH species. The two peaks in the DTA curve located at 367°C and 510°C, respectively, corresponded to the crystallization of the amorphous into anatase phase. Above 600°C, the anatase-rutile phase transition occurred since there was no mass loss in TG curve. Upon Er doping, similar features appeared except Er_2O_3 cubic phase crystallization in TiO_2 film due to requirement of higher ambient temperature. As partial conclusion, Er doping resulted in the softening of V=O bond in V_2O_5 film and O deficit in anatase TiO_2 film. However, keep in mind that Er local structure was determined by the Ti–O arrangement in anatase TiO_2 whereas, in rutile TiO_2, by Er–O chemical property rather than the Ti–O arrangement [7].

Figure 2 showed FTIR spectra of the films in which deconvolution process was applied to identify the IR modes. V_2O_5 films exhibited two large bands at ~1600 and ~3400 cm^{-1}. The peaks between 1400 and 1650 cm^{-1} were OH bending and OH–H stretching from water [8, 9]. Moreover, H_2O and H_3O^+ bonds appeared at 3362 and 3200 cm^{-1}. In the 400–1100 cm^{-1}, the V_2O_5 film exhibited three characteristic vibration modes: V=O vibrations at 1017 cm^{-1} [10], the V–O–V symmetric stretch around 516 cm^{-1} [11], and the V–O–V asymmetric stretch at 756 cm^{-1} [12]. The group of bands presented below 600 cm^{-1} corresponded to the edge sharing 3V–O_C stretching [13] and the bridging V–O_B–V deformations

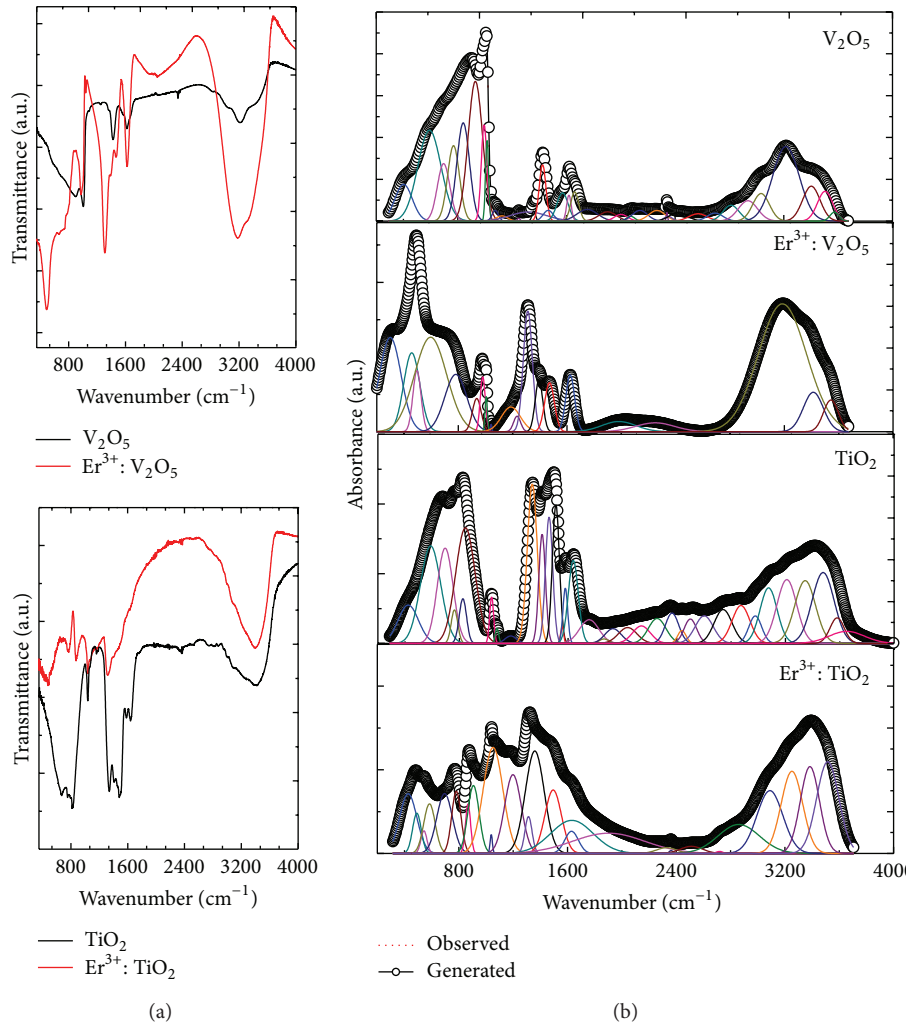

Figure 2: FTIR (a) transmittance and (b) deconvolution spectra of the films deposited on ITO coated glass substrates.

[14]. Peaks at 932 cm^{-1} and 1000 cm^{-1} corresponded to V^{4+}=O and V^{5+}=O bands by indicating nonstoichiometric V_2O_5 film while the band at 830–840 cm^{-1} showed disorder (or amorphous phase) of V_2O_5 film [15]. For TiO_2 film, the presence of Ti–O–Ti and Ti–O polymeric chains was clearly evident from the bands at 471 and 789 cm^{-1}. Also vibration of the Ti–O–O was identified from the band at 693 cm^{-1} [16]. Moreover, the bands at 1009, 1122, and 1138 cm^{-1} were ascribed to stretching of Ti–O–C [17]. LO mode of amorphous TiO_2 [18] appeared at 874 cm^{-1} and the broadband from 3000 to 3600 cm^{-1} associated with the stretching vibration modes of hydroxyl groups [19]. The bands at 1288 and 1368 cm^{-1} were vibration mode of the C–O–O group and the doublet in 1441 and 1538 cm^{-1} designated the symmetric and asymmetric stretching vibration of the carboxylic group coordinated to Ti as a bidentate ligand [17]. Upon Er doping, the bands around 400–450 cm^{-1} corresponded to Er–O bond. Also the huge band at 3000–3500 cm^{-1} was attributed to water related bonds. The bands between 1300 and 3000 cm^{-1} represented the carbon related bonds. Moreover, as deposited, V_2O_5 film showed small peaks at 440 and 600 cm^{-1} that could be assigned to phonon bands of crystallized Er_2O_3 cubic phase [20].

Optical transmittance spectra were given in Figure 3. For V_2O_5 films, transmittance curve is strongly affected by Er doping, causing a blue shift (see the inset of Figure 3(a)) in the optical band gap. Contrary to V_2O_5 films, though no absorption peaks arose in undoped TiO_2 film within visible region [21, 22], absorption peaks related to Er doping in TiO_2 film were observed, located at 490, 523, and 654 nm in absorption measurement (given as inset of Figure 3(a)), and responsible for improvement in photocatalytic activity of TiO_2. E_G's of the films were calculated as to Tauc's law as follows:

$$\alpha h\nu = A(h\nu - E_G)^n, \quad (1)$$

where A was constant, $h\nu$ = photon energy, and n was the fingerprint of the transition. Best fit for all the films was given by a direct allowed transition where $n = 1/2$. V_2O_5 films showed a blue shift with Er doping while TiO_2 films

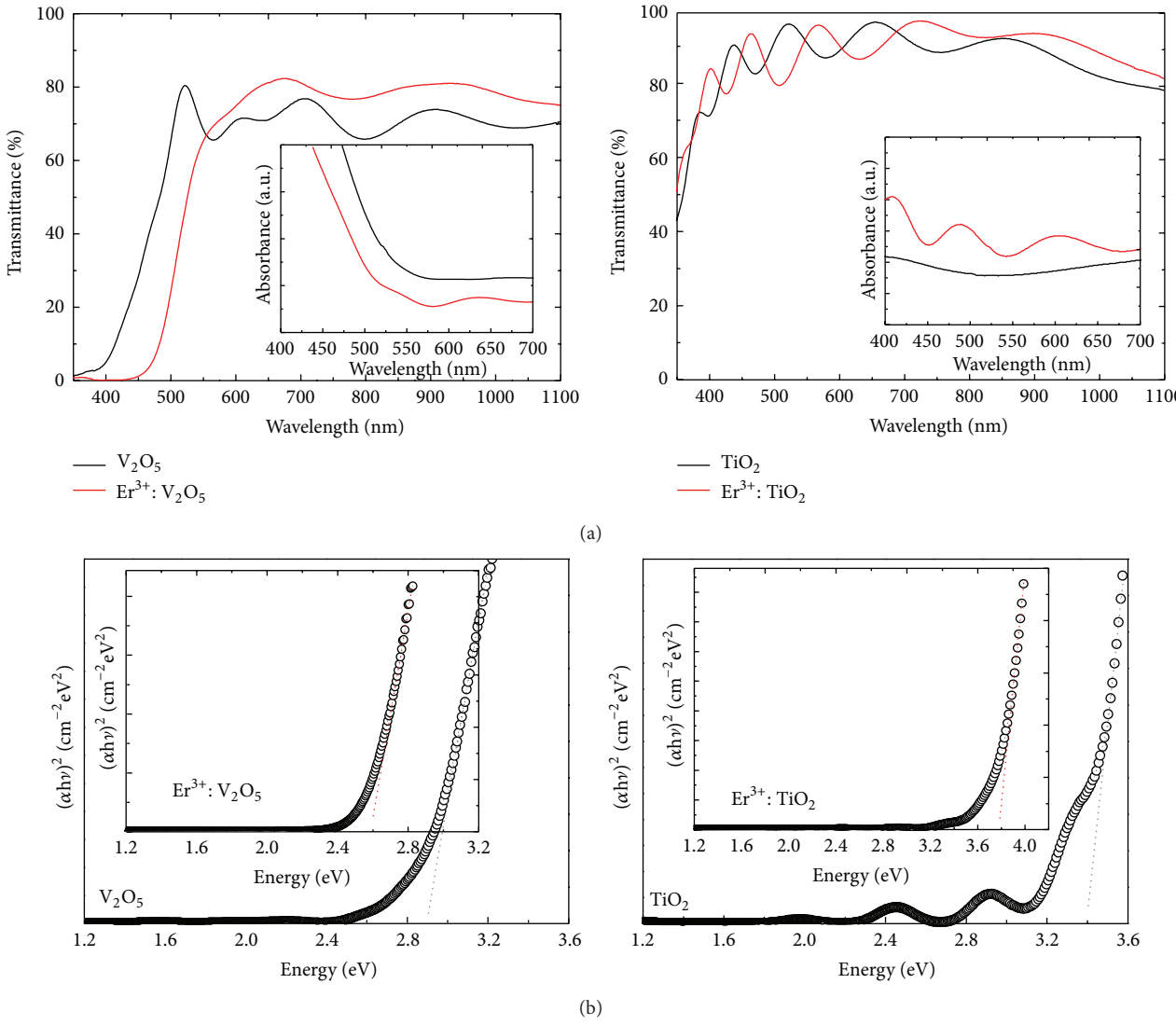

FIGURE 3: (a) Optical transmittance spectra, (b) Tauc plots of the films deposited on ITO coated glass substrates. The inset in (a) demonstrated the absorption measurement whereas in (b) resumed Tauc plot for Er-doped films.

remained almost the same. To verify the formation of Er-doped vanadia/titania films, PL measurements were carried out and depicted in Figure 4. The peaks in the spectra, located at 840 and 980 nm, owing to the transition of $^4I_{15/2} \rightarrow {}^4I_{9/2}$ and $^4I_{15/2} \rightarrow {}^4I_{11/2}$, directly related to Er substitution [23]. Moreover, PL peaks, which appeared at the range of 300–400 nm, was attributed to oxygen vacancy in V_2O_5 film since, due to the weakness of V=O bond, its oxygen was easily removed [24]. In titania films, apart from the peaks emerging in absorption measurement, a slightly shifted and new emerged peaks were present in PL measurement, confirming the successful of Er doping in TiO_2 film [22–25]. Figure 5 displays AFM results of the films. As to the analysis, crack-free and homogeneous films are synthesized and, upon Er doping, the size of the grains increases (decreases) in V_2O_5 (TiO_2) films, similarly to the ZnO:Er films [26, 27]. To ascertain the proposition, X-Ray diffractograms (XRD) were obtained using X-ray diffractometer using CuKα radiation and illustrated in Figure 6. The weak and broad peak around 25° in V_2O_5 film indicated (003) growth direction while, in TiO_2 film, it gave (101) direction with verifying anatase phase [28, 29]. Noteworthily, weaker and broader XRD peaks implied reduced grains size and low extent of crystallinity. Indeed, this was exactly observed in Er-doped TiO_2 film. In V_2O_5 film, relatively strength and narrow XRD diffraction peaks were observed after Er doping. Such results were consistent with the one obtained in absorption measurement on Er-doped TiO_2 and V_2O_5 films. V_2O_5 can exhibit multielectrochromism regarding its layered structure and thickness with the following reaction [30]

$$V_2O_5 + x\left(Li^+ + e^-\right) \longleftrightarrow Li_xV_2O_5 \quad (2)$$

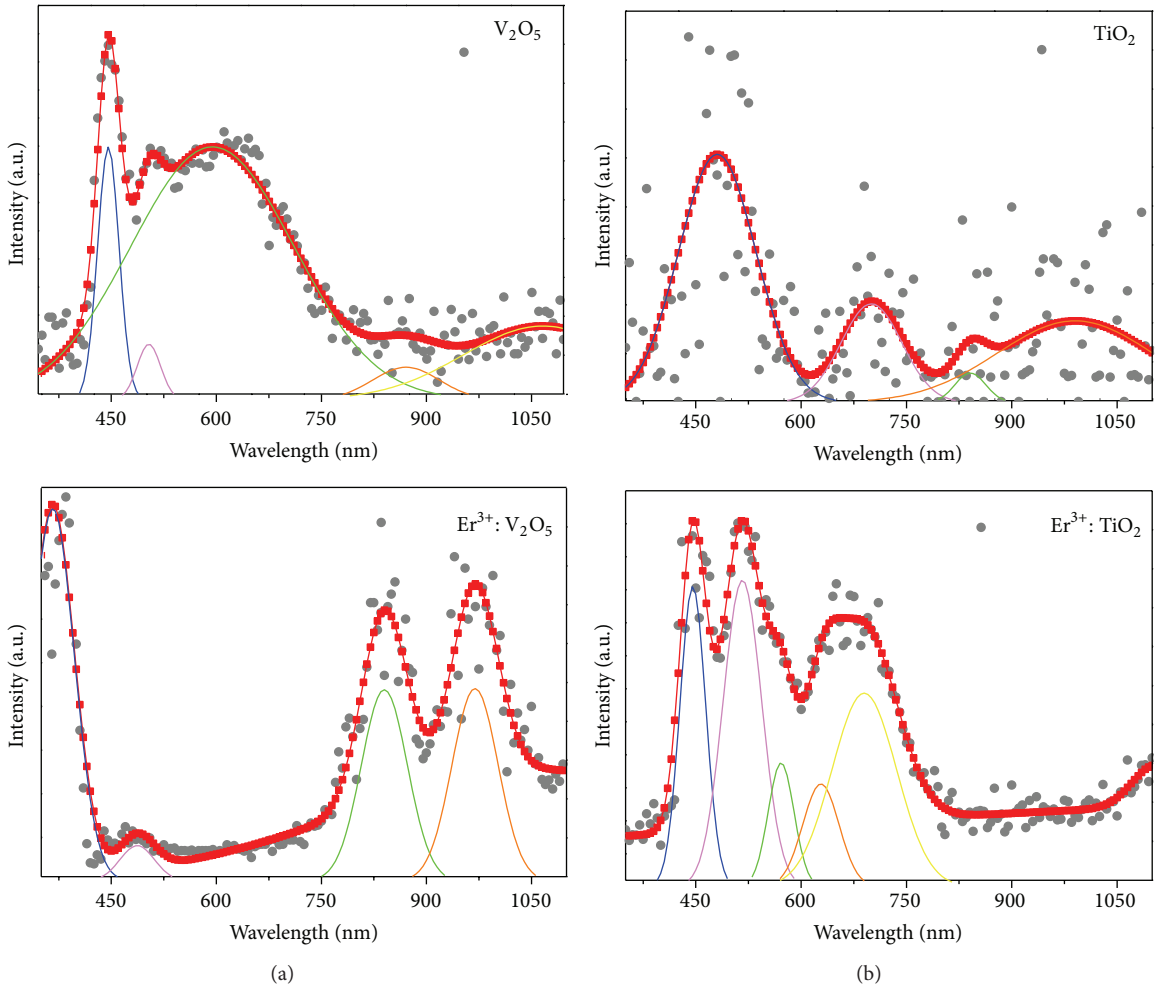

FIGURE 4: Room temperature PL spectra of erbium-undoped/erbium-doped (a) V_2O_5 and (b) TiO_2 thin films.

while TiO_2 shows cathodic electrochromism upon Li^+ and electron insertion into the films with the following reaction [26]:

$$TiO_2 + x\left(Li^+ + e^-\right) \longleftrightarrow Li_xTiO_2 \quad (3)$$

V_2O_5 films demonstrated orange-yellow to green to greyish-blue color with a high contrast while TiO_2 films changed from transparent to greyish-blue color. CVs of the films were illustrated in Figure 7. Anodic: (cathodic) charge capacities upon doping enhanced the charge capacities such that 34.2: (34.2) to 53.1: (53.3) mC/cm^2 for V_2O_5 films while 6.8: (8.2) to 19.7: (29.2) mC/cm^2 for TiO_2 films. The increase was attributed to increasing granule sizes and porosity of the films, verified by AFM measurements. Moreover, Er doping created a blue shift on the band gap values, especially for V_2O_5 films, which might be related to increase in the oxygen vacancies. It was reported that increase of the interlayer distances due to softening of V=O leads to decrease of interlayer interactions and made Li diffusion easier [14]. In Er-doped TiO_2 film, presence of absorption peaks and broader/weaker XRD diffraction peaks suggested a reduction in crystallite size, causing larger surface area. Consequently, it enhanced not only the inserted charge amounts but also the photocatalytic activity.

4. Conclusion

The erbium-undoped/erbium-doped vanadium pentoxide and titanium dioxide thin films were produced via dip coating technique. FTIR and TG/DTA measurements were performed to find out Er substitution. Upon Er doping, UV-Vis spectroscopy indicated a blue shift on the band gap values of V_2O_5 due to the softening of V=O bond. Due to the impact of Er on host material structure, granule size of the V_2O_5 film increased (UV-Vis and AFM measurements) yielding more space for intercalation of ion in host materials. In TiO_2, reduced granule size by Er doping caused increase in surface area and hence dramatic increase in ion storage capacity that were deduced by CV.

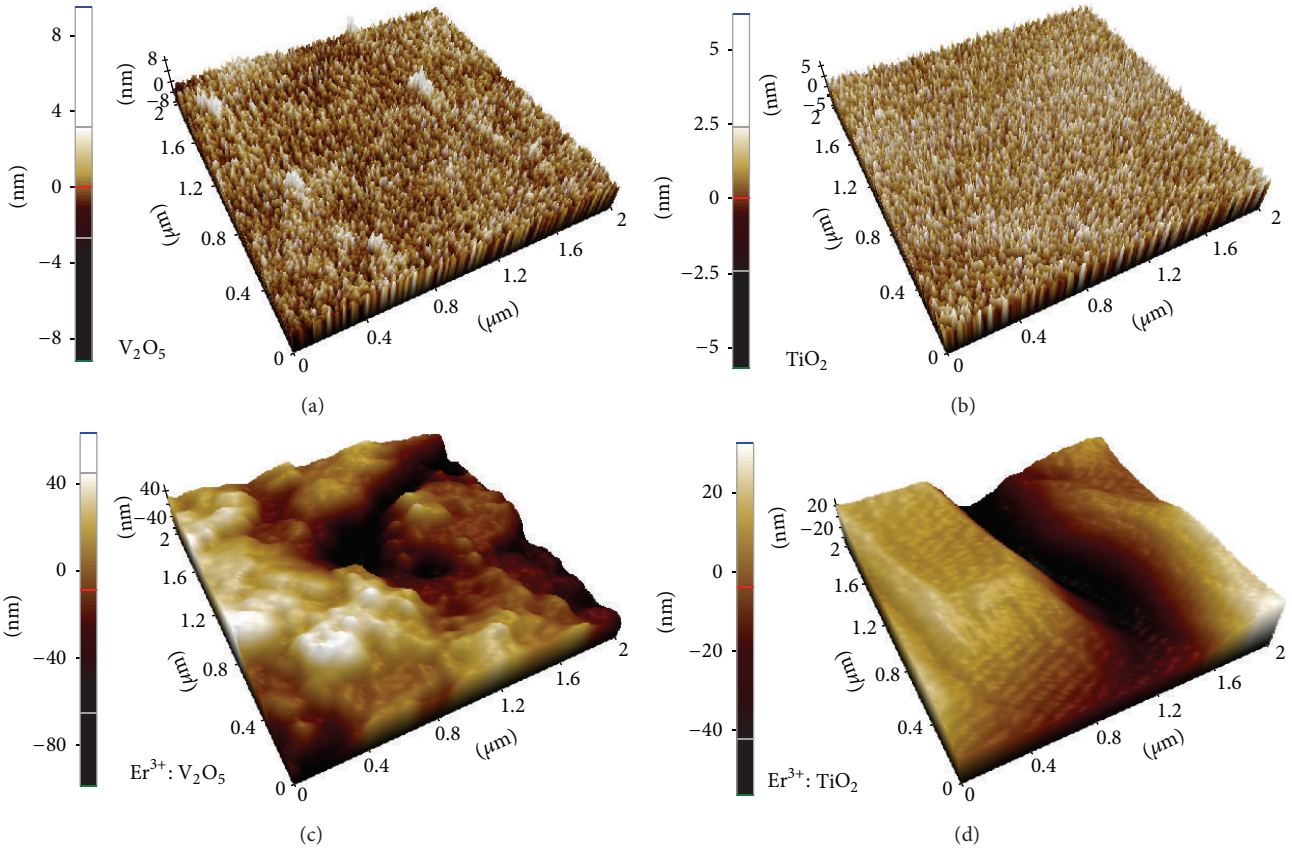

Figure 5: Atomic force microscopy picture of the films deposited on SLG substrates.

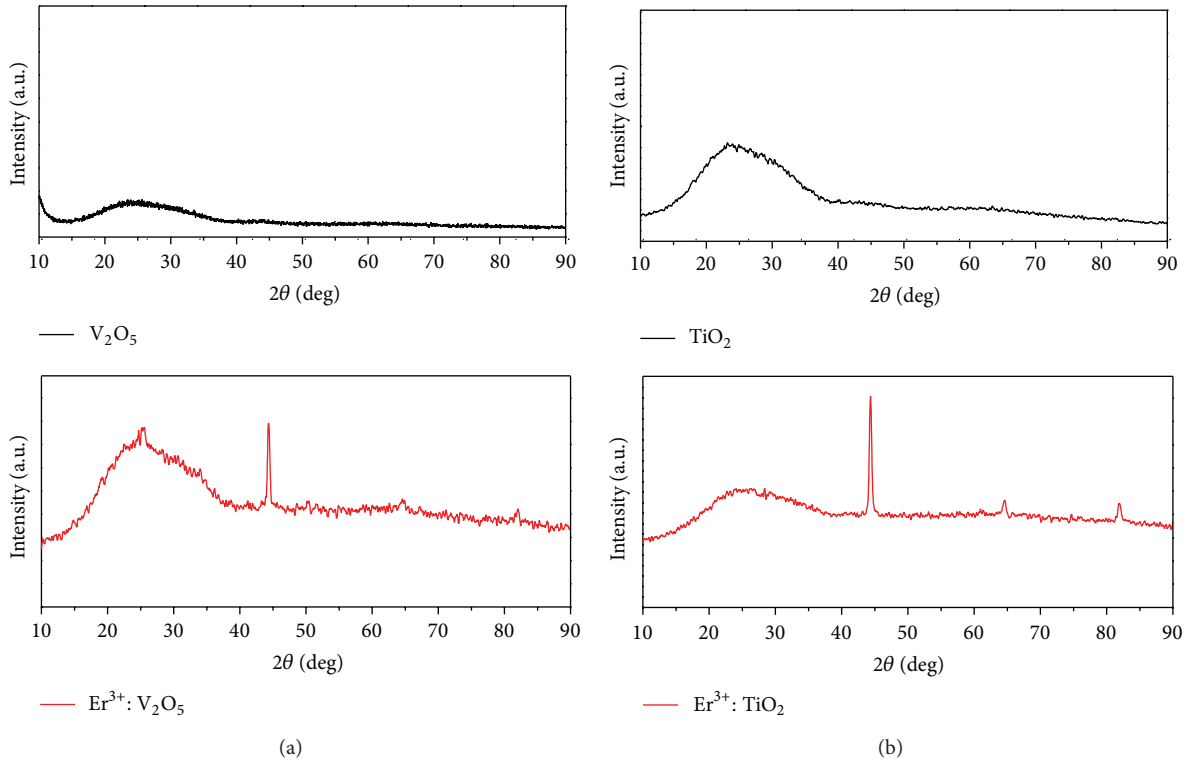

Figure 6: XRD spectra of erbium-undoped/erbium-doped (a) V_2O_5, (b) TiO_2 films.

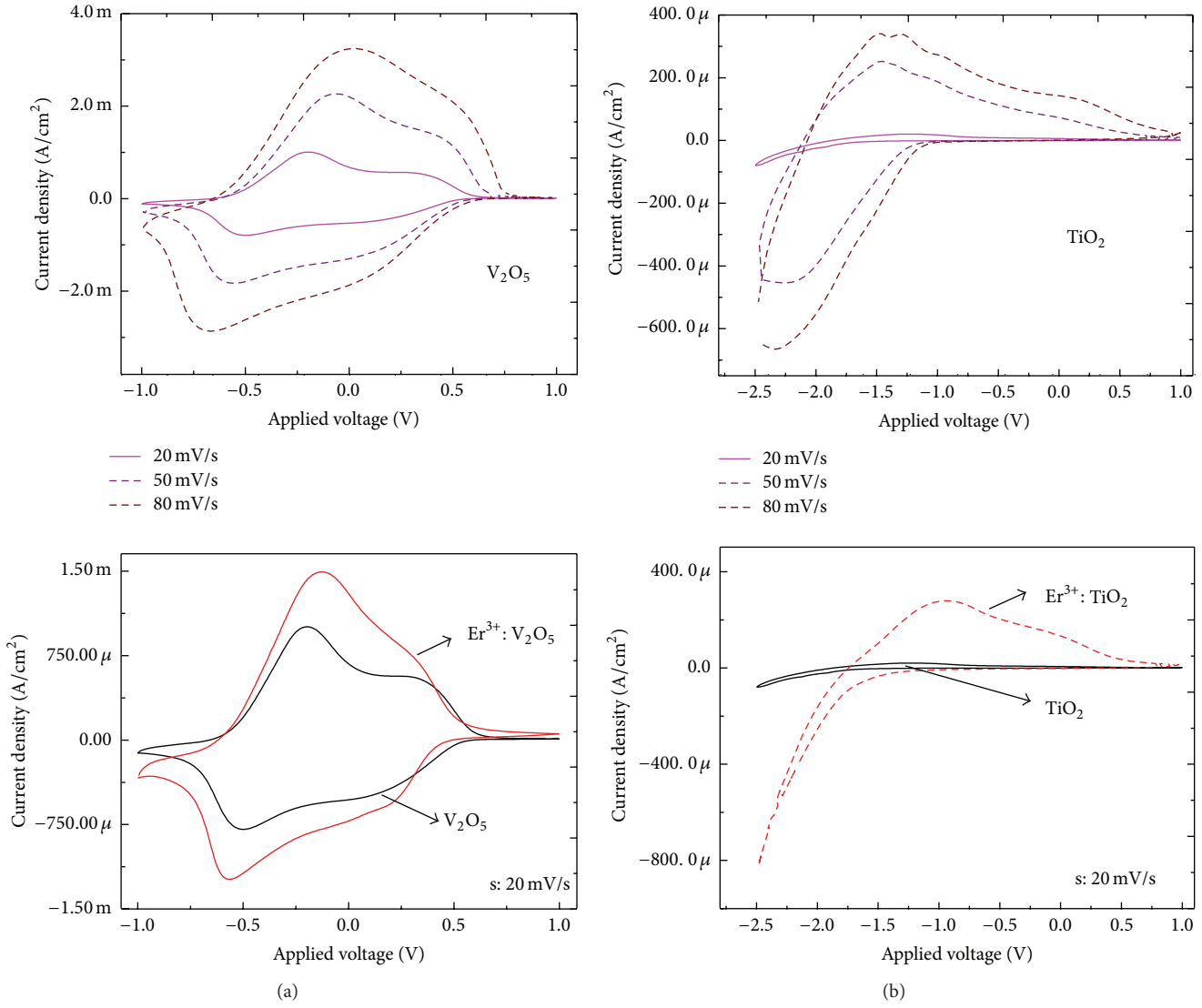

Figure 7: Cyclic voltammograms of the (a) V_2O_5, (b) TiO_2 films at different scan rates.

Conflict of Interests

The authors declare that there is no conflict of interests regarding the publication of this paper.

Acknowledgments

This study is financially supported by Yildiz Technical University projects under Contracts of 2012-01-01-DOP02 and 2011-01-01-KAP03. The authors thank Associate Professor Dr. Nevim SAN for FTIR measurements.

References

[1] L. L. Matskevich and V. V. Bazhinov, "Titanium dioxide optical coatings," *Soviet Journal of Optical Technology*, vol. 44, no. 2, pp. 98–99, 1977.

[2] N. Savage, B. Chwieroth, A. Ginwalla, B. R. Patton, S. A. Akbar, and P. K. Dutta, "Composite n-p semiconducting titanium oxides as gas sensors," *Sensors and Actuators, B: Chemical*, vol. 79, no. 1, pp. 17–27, 2001.

[3] C. Natarajan, K. Setoguchi, and G. Nogami, "Preparation of a nanocrystalline titanium dioxide negative electrode for the rechargeable lithium ion battery," *Electrochimica Acta*, vol. 43, no. 21-22, pp. 3371–3374, 1998.

[4] A. Talledo and C. G. Granqvist, "Electrochromic vanadium-pentoxide-based films: Structural, electrochemical, and optical properties," *Journal of Applied Physics*, vol. 77, no. 9, pp. 4655–4666, 1995.

[5] V. Štengl, S. Bakardjieva, and N. Murafa, "Preparation and photocatalytic activity of rare earth doped TiO_2 nanoparticles," *Materials Chemistry and Physics*, vol. 114, no. 1, pp. 217–226, 2009.

[6] C. Mignotte, "Structural characterization for Er^{3+}-doped oxide materials potentially useful as optical devices," *Applied Surface Science*, vol. 226, no. 4, pp. 355–370, 2004.

[7] M. Ishii, S. Komuro, and T. Morikawa, "Study on atomic coordination around Er doped into anatase- and rutile-TiO_2: Er-O clustering dependent on the host crystal phase," *Journal of Applied Physics*, vol. 94, no. 6, pp. 3823–3827, 2003.

[8] O. Özdemir, F. P. Gökdemir, U. D. Menda, P. Kavak, A. E. Saatci, and K. Kutlu, "Nano-crystal $V_2O_5nH_2O$ sol-gel films made by dip coating," in *Proceedings of the 2nd International Advances in Applied Physics and Materials Science Congress (APMAS '12)*, pp. 233–240, April 2012.

[9] N. Ozer and C. M. Lampert, "Electrochromic performance of sol-gel deposited WO_3–V_2O_5 films," *Thin Solid Films*, vol. 349, no. 1, pp. 205–211, 1999.

[10] V. M. Mohan, B. Hu, W. Qiu, and W. Chen, "Synthesis, structural, and electrochemical performance of V_2O_5 nanotubes as cathode material for lithium battery," *Journal of Applied Electrochemistry*, vol. 39, no. 10, pp. 2001–2006, 2009.

[11] F. Huguenin, M. J. Giz, E. A. Ticianelli, and R. M. Torresi, "Structure and properties of a nanocomposite formed by vanadium pentoxide containing poly(*N*-propane sulfonic acid aniline)," *Journal of Power Sources*, vol. 103, no. 1, pp. 113–119, 2001.

[12] Y. Chen, X. Zhou, X. Zhao, X. He, and X. Gu, "Crystallite structure, surface morphology and optical properties of In_2O_3-TiO_2 composite thin films by sol-gel method," *Materials Science and Engineering B: Solid-State Materials for Advanced Technology*, vol. 151, no. 2, pp. 179–186, 2008.

[13] C. V. Ramana, O. M. Hussain, B. S. Naidu, and P. J. Reddy, "Spectroscopic characterization of electron-beam evaporated V_2O_5 thin films," *Thin Solid Films*, vol. 305, no. 1-2, pp. 219–226, 1997.

[14] M. B. Sahana, C. Sudakar, C. Thapa et al., "Electrochemical properties of V_2O_5 thin films deposited by spin coating," *Materials Science and Engineering B: Solid-State Materials for Advanced Technology*, vol. 143, no. 1–3, pp. 42–50, 2007.

[15] S.-H. Lee, H. M. Cheong, M. J. Seong et al., "Raman spectroscopic studies of amorphous vanadium oxide thin films," *Solid State Ionics*, vol. 165, no. 1–4, pp. 111–116, 2003.

[16] Y. Gao, Y. Masuda, Z. Peng, T. Yonezawa, and K. Koumoto, "Room temperature deposition of a TiO_2 thin film from aqueous peroxotitanate solution," *Journal of Materials Chemistry*, vol. 13, no. 3, pp. 608–613, 2003.

[17] R. Parra, M. S. Góes, M. S. Castro, E. Longos, P. R. Bueno, and J. A. Varela, "Reaction pathway to the synthesis of anatase via the chemical modification of titanium isopropoxide with acetic acid," *Chemistry of Materials*, vol. 20, no. 1, pp. 143–150, 2008.

[18] A. Verma and A. G. Joshi, "Structural, optical, photoluminescence and photocatalytic characteristics of sol-gel derived CeO_2-TiO_2 films," *Indian Journal of Chemistry A Inorganic, Physical, Theoretical and Analytical Chemistry*, vol. 48, no. 2, pp. 161–167, 2009.

[19] D. G. Lewis and V. C. Farmer, "Infrared absorption of surface hydroxyl groups and lattice vibrations in lepidocrocite (γ-FeOOH) and boehmite (γ-AlOOH)," *Clay Minerals*, vol. 21, no. 1, pp. 93–100, 1986.

[20] R. Xu, Q. Tao, Y. Yang, and C. G. Takoudis, "Atomic layer deposition and characterization of stoichiometric erbium oxide thin dielectrics on Si(100) using $(CpMe)_3$ Er precursor and ozone," *Applied Surface Science*, vol. 258, no. 22, pp. 8514–8520, 2012.

[21] J.-G. Li, X. Wang, C. Tang, T. Ishigaki, and S. Tanaka, "Energy transfer enables 1.53 μm photoluminescence from Erbium-Doped TiO2 semiconductor nanocrystals synthesized by Ar/O_2 radio-frequency thermal plasma," *Journal of the American Ceramic Society*, vol. 91, no. 6, pp. 2032–2035, 2008.

[22] D. Y. Lee, B.-Y. Kim, N.-I. Cho, and Y.-J. Oh, "Electrospun Er^{3+}-TiO_2 nanofibrous films as visible light induced photocatalysts," *Current Applied Physics*, vol. 11, no. 3, pp. S324–S327, 2011.

[23] J. T. Torvik, R. J. Feuerstein, C. H. Qiu, J. I. Pankove, and F. Namavar, "Photoluminescence excitation measurements on erbium implanted GaN," *Journal of Applied Physics*, vol. 82, no. 4, pp. 1824–1827, 1997.

[24] M. Anpo, I. Tanahashi, and Y. Kubokawa, "Photoluminescence and photoreductlon of V_2O_5 supported on porous Vycor glass," *Journal of Physical Chemistry*, vol. 84, no. 25, pp. 3440–3443, 1980.

[25] S. Komuro, T. Katsumata, H. Kokai, T. Morikawa, and X. Zhao, "Change in photoluminescence from Er-doped TiO_2 thin films induced by optically assisted reduction," *Applied Physics Letters*, vol. 81, no. 25, pp. 4733–4735, 2003.

[26] M. H. Choi and T. Y. Ma, "Erbium concentration effects on the structural and photoluminescence properties of ZnO:Er films," *Materials Letters*, vol. 62, no. 12-13, pp. 1835–1838, 2008.

[27] J.-C. Sin, S.-M. Lam, K.-T. Lee, and A. R. Mohamed, "Fabrication of erbium-doped spherical-like ZnO hierarchical nanostructures with enhanced visible light-driven photocatalytic activity," *Materials Letters*, vol. 91, pp. 1–4, 2013.

[28] W. Haiyan, Y. Yuetao, L. Xiaojun, and Z. Shuyi, "Study of erbium (III) doped titanium dioxide nanoparticles by photoacoustic spectroscopy," *Journal of Rare Earths*, vol. 28, no. 2, pp. 211–214, 2010.

[29] D. Y. Lee, M.-H. Lee, and N.-I. Cho, "Preparation and photocatalytic degradation of erbium doped titanium dioxide nanorods," *Current Applied Physics*, vol. 12, no. 4, pp. 1229–1233, 2012.

[30] C. G. Granqvist, *Handbook of Inorganic Electrochromic Materials*, Elsevier, Amsterdam, The Netherlands, 1995.